iScience

CellPress
OPEN ACCESS

Article

A Noninvasive Wearable Device for Real-Time Monitoring of Secretion Sweat Pressure by Digital Display

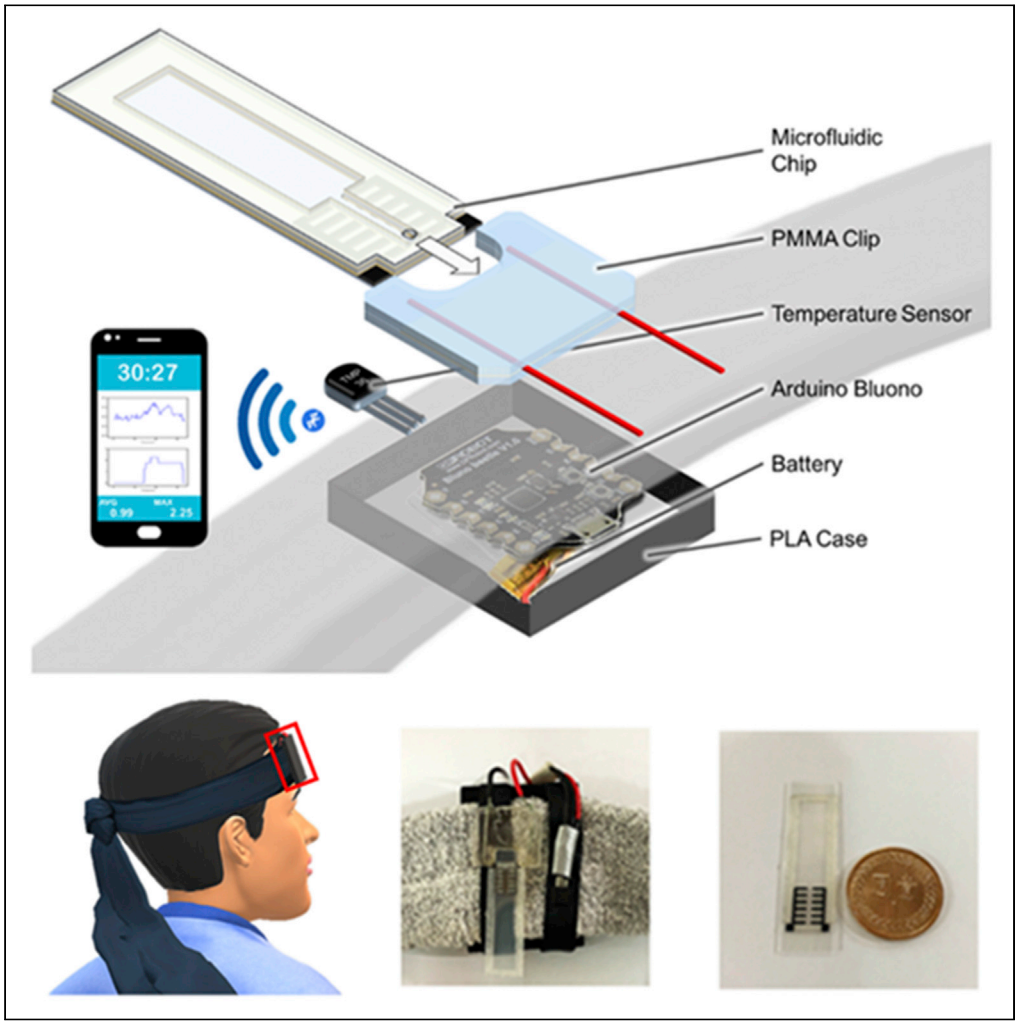

Pei-Heng Lin, Wei-Lun Chang, Sian-Chen Sheu, Bor-Ran Li

liborran@g2.nctu.edu.tw

HIGHLIGHTS

A wearable device sensing secreted sweat pressure for personal health care

A noninvasive method for real-time pressure monitoring displayed on a smartphone

Widely adopted in different individuals for ionic and temperature calibrations

Successful *in situ* measurements with exercise for 30 min

Lin et al., iScience *23*, 101658
November 20, 2020
https://doi.org/10.1016/j.isci.2020.101658

iScience

CellPress
OPEN ACCESS

Article

A Noninvasive Wearable Device for Real-Time Monitoring of Secretion Sweat Pressure by Digital Display

Pei-Heng Lin,[1,2,4] Wei-Lun Chang,[1,4] Sian-Chen Sheu,[1] and Bor-Ran Li[1,2,3,5,*]

SUMMARY

Sweat-based wearable devices have attracted increasing attention by providing abundant physiological information and continuous measurement through noninvasive healthcare monitoring. Sweat pressure generated *via* sweat glands to the skin surface associated with osmotic effects may help to elucidate such parameters as physiological conditions and psychological factors. This study introduces a wearable device for measuring secretion sweat pressure through noninvasive, continuous monitoring. Secretion pressure is detected by a microfluidic chip that shows the resistance variance from a paired electrode pattern and transfers digital signals to a smartphone for real-time display. A human study demonstrates this measurement with different exercise activities, showing the pressure ranges from 1.3 to 2.5 kPa. This device is user-friendly and applicable to exercise training and personal health care. The convenience and easy-to-wear characteristics of this device may establish a foundation for future research investigating sweat physiology and personal health care.

INTRODUCTION

Wearable devices are receiving increasing attraction by giving individual insights into personal physiological information, improving the healthcare quality of life (Liu et al., 2017, 2020; Patel et al., 2012; Ray et al., 2019; Yang et al., 2019). Given the rapid growth of the smartphone population and the improvement of technological developments, a promising solution for simplified wearable devices has been presented. While the sensing component collects physical information from users, it also transports the receiving data to a smartphone application for further processing and real-time display (Lan et al., 2020a; Temiz and Delamarche, 2018; Yao et al., 2019). Numerous skin-attached wearable systems are available in the research field and in commercial products at present, including body temperature detection (Yang et al., 2015), blood pressure (Zheng et al., 2014), sweat (Nakata et al., 2017), and electrocardiography sensing systems (He et al., 2019, 2020; Lan et al., 2020b; Xia et al., 2018). All of these systems have physiological value in establishing a baseline for a personalized healthy equilibrium, indicating the physical condition of the users. The real-time readings provide early warnings for variance of pathology and improve athletic performance for personal fitness. This envisioned healthcare landscape implies continuous point-of-care sensing and personalized prediction, preventing physiological conditions (Kumari et al., 2017; Lin et al., 2020).

Sweat contains a wealth of information in terms of both physical and chemical properties, indicating the deeper physiological dynamic state (Choi et al., 2018; Gao et al., 2016; Sonner et al., 2017). Compared to other biofluids, including blood, interstitial fluid, tears and urine, sweat analytes are generated noninvasively, facilitating easy collection from a convenient location on the body that is ideal for continuous monitoring (Bariya et al., 2018; Corrie et al., 2015; Heikenfeld et al., 2019; Yang et al., 2020). Sweat sensors are placed close to the epidermal area, which benefits immediate detection. These sensors quantify ions and molecules, including sodium (Schazmann et al., 2010), glucose (Lee et al., 2017), uric acid (Yang et al., 2020), and lactate (Anastasova et al., 2017). The variance in these molecules indicates the physiological dynamic state with unbalanced equilibrium and chronic diseases, such as diabetes and gout (Livingston, 2010; Taylor et al., 2009). This variance can also indicate acute problems, such as dehydration, during real-time monitoring. Sweat is generated by the variance of osmolality between plasma and sweat. The ion concentration in sweat is higher than that in plasma, driven by fluid flowing into the sweat gland, subsequently

[1]Institute of Biomedical Engineering, College of Electrical and Computer Engineering, National Chiao Tung University, Hsinchu, Taiwan

[2]Department of Electrical and Computer Engineering, College of Electrical and Computer Engineering, National Chiao Tung University, Hsinchu, Taiwan

[3]Center for Emergent Functional Matter Science, National Chiao Tung University, Hsinchu, Taiwan

[4]These authors contributed equally

[5]Lead Contact

*Correspondence: liborran@g2.nctu.edu.tw

https://doi.org/10.1016/j.isci.2020.101658

transporting the sweat to the surface of the skin (Baker, 2017; Baker, 2019; Christopher H. Gibbons, 2012; Sato et al., 1989). Considering the importance of eccrine sweat gland activity, varied research has focused on the changes of chemical agents, while physical features of sweating have not been fully elucidated due to the inadequacy of proper metrology methods.

Sweat pressure measurement first took place in 1969 by Schulz et al. (Schulz, 1969). These researchers measured the fluid pressure by inserting a micropuncture into the sweat gland duct, enabling them to monitor the secretory pressure while subjects were induced to sweat through introduction of pilocarpine into the skin with an iontophoresis strategy. This invasive method detects single sweat gland values of internal pressure that are significantly different in individuals, ranging from 3 to 70 kPa with 40 kPa as a mean value. Single gland measurement observed the sweat secretion mechanism. However, the medical approach strategy of sweat pressure measurement is not easy to apply in daily health care, as it involves uncomfortable and invasive insertion followed by the use of bulky equipment. Rogers and his research group first coopted a microfluidic system for sweat pressure detection, presenting a noninvasive, soft, skin-mounted microfluidic device for sweating pressure measurements (Choi et al., 2017). This microfluidic system arrays 12 inlets that can detect different sweat pressures through capillary force. A visual color change in the device occurs while the sweat pressure exceeds the set capillary bursting force and flows into the indicator area. This change shows the maximum secretory pressure during the entire exercise with a clear indicator. This advance combined with soft material and a skin-interfaced platform demonstrated a portable, convenient platform that measures the secretory sweat pressures with noninvasive and simple operation. These works inspired us to develop pressure measurement in human sweat. We attempt to establish a noninvasive, portable device for real-time sweat pressure measurements with a smart system to achieve convenient examination for users at any time or place.

In this work, we reported a noninvasive, portable, wearable device that provides real-time sensing of human sweat pressure with body temperature detection. The chip contains a microchannel with six pairs of comb-shaped carbon electrodes and a sealed chamber with only a single inlet connected to the microchannel but no exit. The key concept of such a device is that the sweat attempts to flow into the microchannel, and it is positioned at the location where secretory pressure is applied. The position of the sweat fluid is detected through the resistance variance, and the result is transported to a smartphone system for calibration and calculated into epidermal secretory pressure. Surface temperature is also monitored on the wearable device to assist in calibrating thermal differences of the sealed chamber during the expansion and contraction of the microfluidic chip. A simple platform was established based on this concept and applied to human subjects. Such real-time measurements allow us to monitor the pressure variance and trend during exercise.

RESULTS

Design of the Secretion Sweat Pressure Sensing Integrated System

The sweat pressure sensing device developed in this study is composed of several modules in the integrated system. This wearable device is placed on the forehead area (Figure 1A) of the subject and fastened with a headband. The entire device is in a small volume with approximately 16 g weight, and an image of the system and replaceable microfluidic chip are shown in Figure 1B. Figure 1C illustrates the noninvasive, sweat secretory monitoring device with microfluidic chip and integrated electrode that transports recording data to a personal smartphone. The wearable device comprises a replaceable microfluidic chip, temperature sensor, a battery, and a transmitting device that is continuously tracking the portable device and transports the detected pressure to a smartphone via Bluetooth. Before a new exercise session is begun, a new microfluidic chip is loaded on a PMMA clip that connects to the other modulus. A microcontroller coordinates the information from the detection modulus, sending it to the personal smartphone for further calculation and display of results. The entire sensing platform is integrated into a common headband that can be comfortably worn for collecting sweat in the forehead area without interference during continuous fitness monitoring. Design and implementation of the microcontroller is shown in Figure 1D. The simplified circuit and basic operation principle of the connection in the wearable device are designed for resistance measurement. The Beetle microcontroller connects both the microfluidic chip and temperature sensor with a 3.7 V lithium polymer battery supplying an input signal. A bipolar pulse wave is applied from a digital pin (d5) to the unknown resistor and an 8.2 V voltage divider. With continuous monitoring by A1, the resistance voltage is differentiated to six pressure degrees and displayed on the smartphone every 8 s.

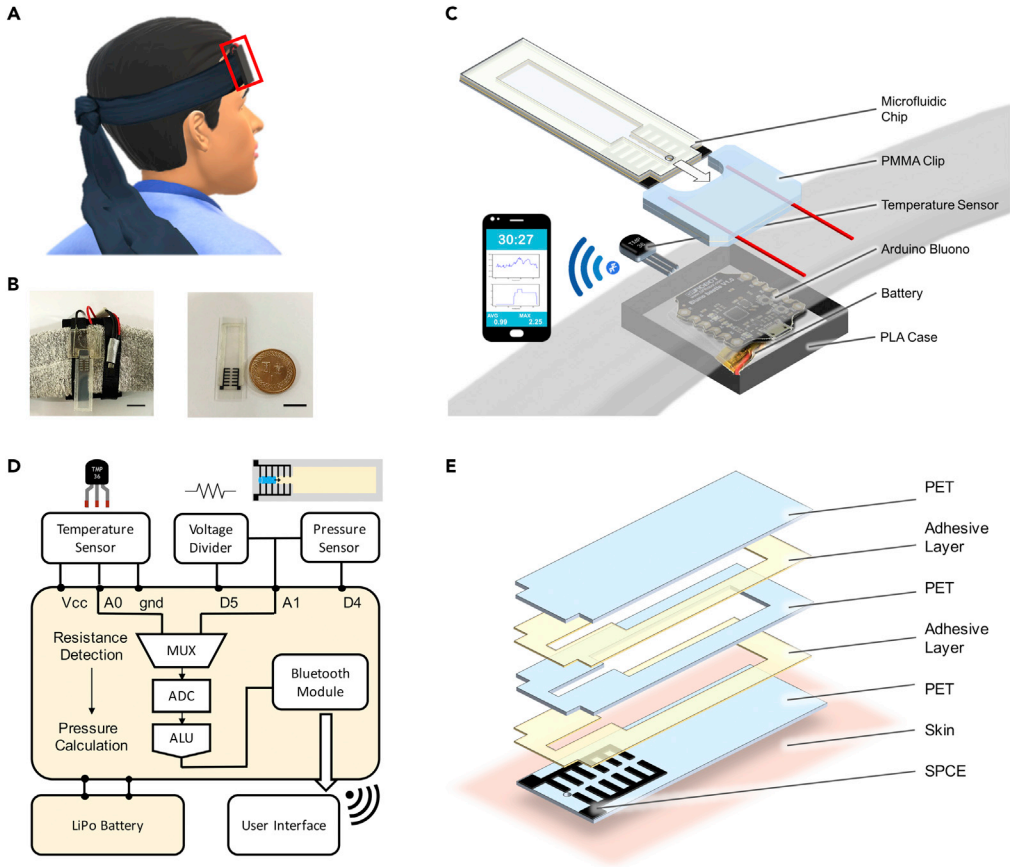

Figure 1. Schematics of the Wearable Secretion Pressure Device for Human Sweat Monitoring

(A) The wearable device is located on the forehead area for sweat detection and fastened by a headband.

(B) Photographic image of the easy-to-carry system and the replaceable microfluidic chip. The scale bar represents 10 mm for the insert.

(C) 3D rendered image of the wearable device that measures the sweating pressure by microfluidic chip and sends the data to a smartphone via Bluetooth.

(D) Circuit and basic operation diagram showing the signal transduction, processing and wireless transmission from the sensor to user interface.

(E) Schematic diagram of the microfluidic chip, from the bottom layer in contact with the skin interface to the top layer.

The main detecting modulus including a temperature sensor and pressure sensing microfluidic chip is the key component in our device. The microfluidic chip consists of five layers of pressure sensing (Figure 1E) composited in a microchannel and a sealed chamber. This chip is designed and fabricated mainly from the material polyethylene terephthalate (PET). The bottom layer plays an important role in attaching to the epidermal surface for sweat collection through a single inlet. Six pairs of comb-like screen-printed carbon electrode electrodes (SPCEs) were located along each side of the microchannel, offering accurate measurement of the pressure degree. A microchannel and sealed chamber is patterned in the middle layer with a third layer added on the top. For further reinforcement of the stability of the microfluidic sensor, additional epoxy resin is properly coated on the edge of the microfluidic device to avoid air loss in the sealed chamber.

Design of the One-Inlet Pneumatic Microfluidic Chip for Secretory Pressure Measurement

The microfluidic conduction of the compression of trapped air and liquid applied pressure in order to measure the secretion pressure of human sweat. The sensing system is tightly attached to the forehead skin of the subject. Secretion sweat under pressure is applied to the single inlet, and liquid is forced to enter the microchannel, thereby compressing the air inside. Since the composition of sweat contains abundant charged ions, such as sodium, chloride, and potassium, the position of the liquid changes the resistance

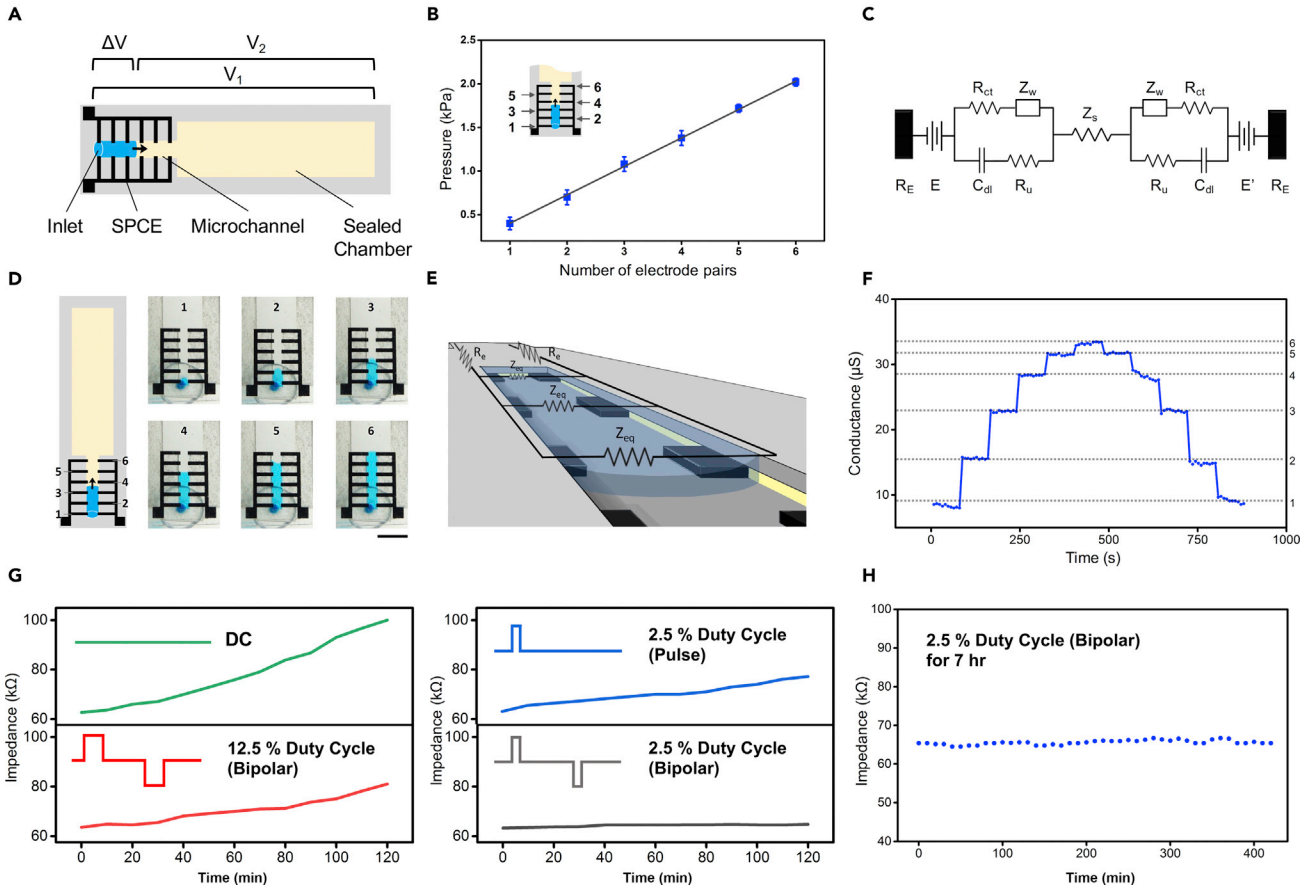

Figure 2. Characterization of the Pressure Sensing Microfluidic Chips

(A) The schematic of secretion pressure measurement of the microfluidic chip.

(B) Response of the pressure value in the microchannel location.

(C) Shows the simplified circuit diagram in microfluidic chip.

(D) Flow monitoring for different numbers of electrode pairs. The scale bar represents 5 mm for the insert.

(E) Illustrates the pressure monitoring system through flow positioned with longitudinally partnered electrode pairs.

(F) The plot showing the resistance value measured through each electrode pair.

(G) Different applied signal through G impedance variance with different input applied.

(H) Impedance stability with bipolar signal applied.

between two teeth of the electrodes, while sweat flowing through two parallel electrodes is caused by sweat in place. The measurement concept is shown in Figure 2A. Initially, air at atmospheric pressure (P_{atm}) is trapped inside the sealed chamber and microchannel with original volume V_1. While sweat migrates to the single inlet, it starts to compress the air inside. As the liquid enters the microchannel through applied pressure (P_{sweat}), we assume the volume of the air in the sealed chamber decreases (V_2). With no air escaping, the molarity (n) of the air still remains the same. Therefore, based on the ideal gas law, P_{sweat} can be deduced through variance of the air volume (ΔV), where temperature (T) and molarity (n) are constant in the equilibrium state.

$$\Delta V = V_1 - V_2 = \frac{V_2(P_{sweat} - P_{atm})}{P_{atm}} \quad \text{(Equation 1)}$$

In this equation, P sweat is the applied secretion pressure. ΔV is the variance of the trapped air volume that can be calculated by the original volume (V_1) and the compression volume (V_2). P_{atm} is defined as 1013.25 kPa under a 25°C environment. As a demonstration, we have measured the changes of the trapped air volume and the applied pressure to mimic real application. The result of the fabricated microfluidic system is presented in Figure 2B; while the applied pressure increases, the variance of the air volume also increases. The compression degree of the trapped air decides the flow liquid location.

Design of the Implemented Electrodes and Electronics for Real-Time Sweat Pressure Monitoring

The concept of liquid measuring relies on the change of resistance across two parallel SPCE that are gradually wetted by advancing secretary sweat along the microchannel flow path. We adopted a widely used equivalent circuit model in order to analyze the resistance response (Figure 2C). The bipolar current can be passed between an electrode-electrolyte interface. Such disparity can be described in a charge-transfer resistance (R_{ct}) or a faradaic leakage resistance. The double layer capacitance (C_{dl}) is parallel to the R_{ct}. Where Z_S represent solution impedance. R_E and R_u are the impedance of the electrode and electrode interface, respectively. A half-cell potential is related to every electrode immersed in solution (E, E′). The limitations of the electrolytes mass transportation called Warburg impedance (Zw) for partial diffusion control.

The detecting SPCE is printed on the bottom layer of PET with a width of 0.5 mm. A set of comb-like electrodes was positioned along of the microchannel, and 6 electrode pairs are patterned orthogonal to the flow direction. A pulse-width bipolar voltage is applied on both sides of the electrodes for resistance measurement. In this case, the design can effectively minimize the electrochemical reaction between electrodes and electrolyte interface in secretary sweat. The illustration of pressure sensing using printed electrodes in a microfluidic chip is shown in Figure 2D. In the initial stage of exercise, when sweat is not adequate enough to enter in the microchannel, the SPCE remained an open circuit since there is no electrolyte connecting both sides of the electrodes to form a circuit loop. After exercise for a short while secretion pressure increased, and the sweat fluid entered into the microchannel. When liquid wets the electrode, an interface resistance forms at the liquid-electrode interface in electrode pairs. Such a liquid-electrode interface causes a resistance signal change that is able to be detected by the microcontroller. According to the high and low during the sweat pressure changes, the wetted electrode pairs provide different resistance signals to the microcontroller for pressure value determination. The following equation describes the connection in the first paired electrode. According to the connections between different electrode pairs, a well-established equivalent for resistance detection in first paired electrode is shown below.

$$R_1 = 2R_E + 2[(R_{ct} + Z_W)//(2R_u + \frac{1}{jwC_{dl}})] + \frac{E' - E}{I} + Z_S \quad \text{(Equation 2)}$$

The equation describes the wetted first paired electrode (R_1). According to the fixed distance between paired electrodes, the equivalent can be derived into the following formula.

$$R_{tot} = 2R_E + \{2[(R_{ct} + Z_W)//(2R_u + \frac{1}{jwC_{dl}})] + \frac{E' - E}{I} + Z_S\}/n \quad \text{(Equation 3)}$$

where n is the number of connected paired electrodes. Across two electrodes, dielectric capacitance C_{dE} is considered to be parallel to the R_E–C_{dl}–R_S–C_{dl} –R_E branch but is in an inactive state, where the given frequency of the voltage source in this study is notably low. In Figure 2F, artificial sweat is injected into the microchannel and recorded through our monitoring system. We gradually increased the applied pressure against the inner pressure in the sealed chamber, allowing fluid to pass through the microchannel. The regulated fluid advanced forward through the paired electrodes one after another. Fluid stayed in each paired electrode for 80 s. According to this result, when fluid passes through different numbers of paired electrodes, certain resistance value can be detected. The signal in each interval is stable in both forward and backward movements. Therefore, the resistance detection can be transformed into pressure values reliably. In this sweat detecting model, we adopted an AC signal in order to avoid the accumulation of high voltage on the electrode resulting in the increase of impedance (Figure 2G). The bipolar signal of 2.5% duty cycle shows the long-term stability in impedance variance lasting for over 7 hr (Figure 2H).

Characterization of Sweat Pressure Sensing Chip in Different Biological Environments

Many studies have shown the composition of human sweat varies substantially among individuals (Taylor and Machado-Moreira, 2013). Changes in ion concentration (Ranchordas et al., 2017) and pH value (Coyle et al., 2009) might affect the outcomes of a pressure sensing system. While the resistance of the fluid in the microchannel increases, it is also a proportional change when detecting resistance results, interfering in the determination of which paired electrodes have been connected. For the purpose of calibration to individual differences in pressure measurements, different ion concentrations are tested in the wearable device. In this study, we chose 3 different concentrations of sodium, which is the primary ion in sweat, as the low, high, and middle values of sodium concentration in human sweat, and the results are shown in Figure 3A. The final detected resistance is proportional to the resistance of artificial sweat. Each number of paired

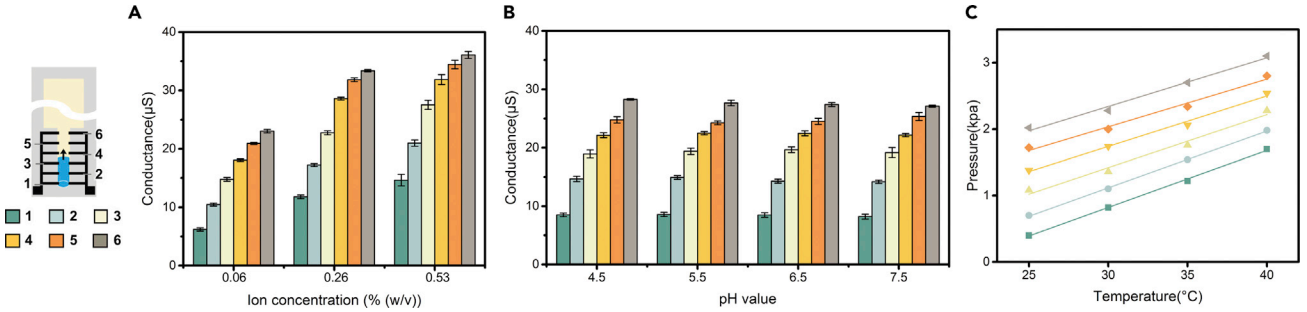

Figure 3. Characterization of the Secretion Pressure Sensing System

(A) Representative responses of three different ionic concentrations in flow detection.

(B) Resistance variance in different electrode pairs in varied pH value artificial sweat.

(C) Plot showing the resistance gradient trend depends on the thermal condition.

electrodes from 1 to 6 showed an orderly increase distributed from 6.2 to 36.1 μS under 0.06–0.53% (w/v) sodium concentration.

Additionally, different pH values of sweat fluid were considered in this study, and the results are shown in Figure 3B. The conductance change in pH value between 4.5 and 7.5 is distributed from 8.2 to 28.3 μS. The result reflects the limitations of pH value to alter the conductance response across the electrode pairs; hence, the sweat-sodium concentration dominates the conductance response compared to the pH value in human sweat. In both the ion concentration and pH value test, acceptable standard deviation in conductance caused by the tiny movement of the liquid-air interface wavering on the same paired electrode were observed. Without observing different paired electrode overlapping with each other under the same solution condition, we partitioned the conductance response into 6°, reflecting 6 pressure values. As sweat fluid flowed into the channel and a reasonable initial response was detected, resistance of the solution (R_s) can be calculated through Equation (2). The following range of each conductance degree can be deducted based on Equation (3) in order to identify the correct pressure under different solution conditions.

Additionally, we considered the thermal drifting effect in microfluidic chip detection, as well. The air in the sealed chamber changed under different temperatures due to the physiological body temperature or the environmental condition. Air could expand in the sealed chamber experiencing a higher temperature environment that added extra contented force for the applied fluid. Figure 3C shows the pressure response of each paired electrode at 25°C–40°C. The detection range of applied pressure is 0.4–2.02 kPa at 25°C, while the range increases to 1.7–3.1 kPa at 40°C. For each electrode pair, higher pressure is required to locate in the same position under higher temperature. The pressure sensitivity was characterized with high signal linearity of $R^2 = 0.9917$. The pressure required (to reach the same teeth of the electrodes) linearly increased as the thermal changes around the microfluidic chip varied from 25°C to 40°C. In view of the average normal temperature of forehead drifting between 35°C and 37°C (Choi and Loftness, 2012), we applied the linear characteristic to calibrate the pressure degree after conductance data was converted and obtained the final real-time sweat pressure results of users.

In situ Measurements of Sweat Pressure Sensing System in Human Subjects

In situ body testing involved evaluations with four healthy adult volunteers who wore the sweat pressure monitoring system during three different types of exercise (jogging, badminton, and spinning bike). The wearable device is attached to the middle area of the forehead on subjects, fixed by a sport headband. The site was chosen for its combination of a reasonably high density of sweat glands (155 glands per cm^2) and high sweating rate (ranging from 697 g m^{-2} h^{-1} to 1710 g m^{-2} h^{-1}) during exercise (Smith and Havenith, 2011; Taylor and Machado-Moreira, 2013). Additionally, in this position with a fastening headband, subjects can comfortably wear the device with minimal movement obstruction during activities.

The studies included the device mounted on the forehead with pressure measurements for 30 min in each scenario. In every human test, the sweat pressures corresponded during the exercise process. At the final stage of each session, subjects rested for a while and the secretion pressure slowly decreased back to

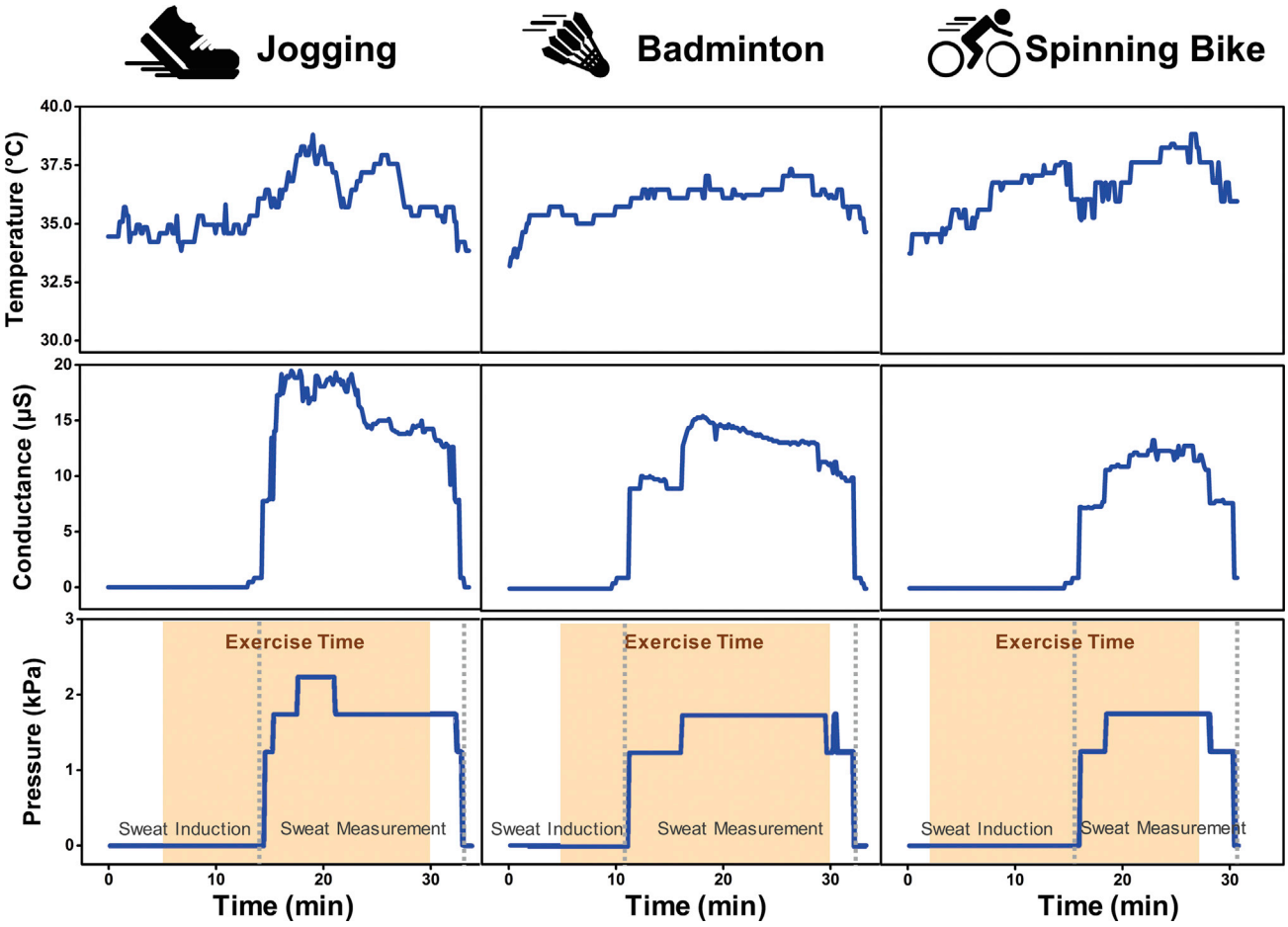

Figure 4. In Situ Measurements of Pressure Sensing Wearable Device During Different Exercise Processes

Measured pressures from three different conditions (jogging, badminton and spinning bike). The thermal condition, resistance value and the adapted pressure result are shown in the real-time display.

baseline through reabsorption, which is a reversal of the steps of sweat production during the accumulation of sweat (Taylor and Machado-Moreira, 2013). The data were recorded since the beginning of the activity, including temperature and resistance values. With the single inlet of the detection microchannel attached to the forehead area tightly, the sweat flows into the channel after a while. The change of the conductance is received by the microcontroller that transports data to the user smartphone for real-time calculation and displays body temperature, resistance and secretary sweat pressure (Figure 4.). Affected by multiple variables such as individual physical conditions and activity intensity, the composition of sweat causes a signal deviation in conductance. Additionally, the environmental temperature disturbs the actual pressure sensing. As a result, the sensing pressure setup was readjusted by the first resistance change in the wetted electrode pairs and actually revised with dependence on environmental temperature. The adapted result is presented in the final secretion pressure. In the sweat induction state, no variance of resistance signal is detected, and the secretion pressure remains 0 kPa. Over approximately 10 min, the real-time monitoring records the actual feedback on the secretion pressure. The outputs showed rises and falls in the sensing pressure that might related to the intermittent exercise and short rest intervals. The highest pressure is detected in the jogging test with a maximum value at 2–2.5 kPa. In the badminton and spinning bike tests, the monitoring value stays under 2 kPa.

Figures 5A, 5B, and 5C show the on-body testing of the wearable device on different volunteers during jogging, badminton, and spinning bike. The wearable system is integrated together and located on the forehead area. In each type of exercise, with different exercise intensity, outer environment and movement

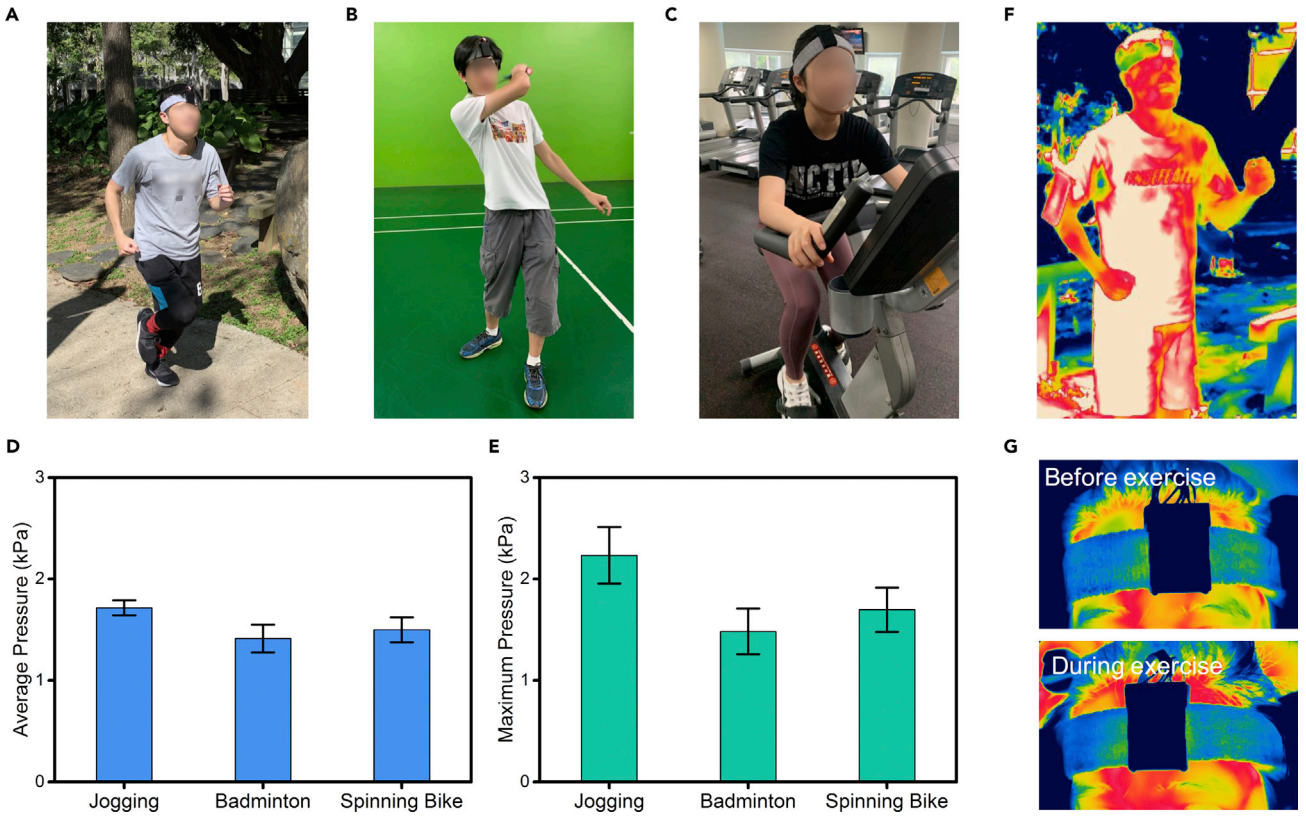

Figure 5. Status and the Detection Results of in Situ Trials

The images present the different exercise situations with (A) (jogging), (B) (badminton), and (C) (spinning bike).

(D) shows the plot of average sweat pressure values during different exercises.

(E) presents the maximum value of the secretion pressure in different exercises.

(F) Infrared imaging of the jogging trail.

(G) Close-up infrared image of the before and after exercise process on the forehead area.

behavior, the output signal slightly differs from that of others, and the data are shown in Figures S3–S5. The average speed in jogging was controlled between 5 and 9 km hr^{-1} with no pulse, resulting in an average pressure of 1.74 $\pm$ 0.1 kPa (Figure 5D). In the spinning bike test, the speed was set between 30 and 50 km hr-1 in every subject with an average pressure of 1.5 $\pm$ 0.12 kPa. During the badminton activity, the average pressure showed the lowest average at 1.42 $\pm$ 0.14 kPa. In Figure 5E, the maximum secretion value ranges from 2.5 kPa to 1.3 kPa. The highest maximum pressure is detected in jogging, which might be due to the continuous active movements and hot environment compared to other exercise. In these experiments, the air temperature and the exercise intensity dominated the secretary pressure of sweat, and the measured conductance value remains steady without sudden pulses throughout the whole process.

The infrared images of subjects during exercise trials are shown in Figures 5F and 5G. The infrared images showed the temperature distribution across the body and forehead area of subjects where white and red represent high heat, and green and blue mean low temperature. The localized heating in the vicinity of the forehead area increases the temperature after exercise.

DISCUSSION

We demonstrated a user-comfortable wearable device for noninvasive, continuous monitoring of the secretion sweating pressure using resistance variance. The device was composed of a disposable microfluidic chip and other reusable electronics, including thermal sensors, microcontroller and rechargeable battery, and it is highly suitable and adaptable for real-time pressure measuring during exercise training applications in personal health care. Pressure monitoring uses wetted paired electrodes that are in contact

	Micropuncture	Soft Microfluidic Devices	This Study
Development year	1969	2017	2020
Detecting method	Intrusive	Noninvasive	Noninvasive
Sweat	Internal pressure	External pressure	External pressure
Equipment size	Large	Small	Small
Device type	Clinical research	Wearable device	Wearable device
Presented result	Physical calculation	Visual recognition	Digital signal
Measuring time	Real-time	Single measurement	Real-time
Reference	(Schulz, 1969)	(Choi et al., 2017)	This study

Table 1. Comparison of Sweat Pressure Measurement Devices

with sweat liquid. The liquid location reflects the applied pressure degree from the inlet. In a reasonable range of sweat pressure measurement, the detecting device can easily enhance the sensitivity by increasing the number of paired electrodes. Additionally, the detecting pressure range can be adjusted through the ratio of the volume between sealed chamber and microchannel. Regarding the measuring location, the wearable device is not restricted to the forehead area and can be applied to other regions of the body, such as the upper arm and back, in consideration of lowered irritation or discomfort obstruction in activity for a comfortable location (in Supporting information S2 and Table S1). With simple operation, this easy-to-wear system is more user-friendly for general users that can monitor their physical condition through digital signals and record it on a smartphone.

However, such a convenient device still faces several challenges. (1) Current sweat-related wearable devices face the problem of the lack of correlation between sweat and a particular health condition. (2) Very little research has developed the secretion pressure of human sweat sensors, and it is difficult to compare (Table 1). Given the lack of suitable metrology methods, the physical characteristics of sweat have not been studied clearly. The sweating pressure is generated by eccrine sweat glands due to the osmolality difference between sweat and blood, indicating that sweat pressure might represent certain orientations of physical condition, similar to blood pressure. Despite the fact that the physical information about sweat is still vaguely related with physiological condition, sweat provides great promise in noninvasive, on-demand, and convenient collection for continuous monitoring over other biofluids. These advantages make sweat measurements more applicable and acceptable for the general public to comfortably measure the body dynamic state constantly. Given the rich physiological information, sweat measurements are conceivably alternatives to blood analysis, cooperate with other molecular detection methods, and have great potential to approach the forefront of wearable technology innovation. The development of such a convenient device combined with electrochemical sensing(Lin and Li, 2020), biomarkers, and big data provides the opportunity for comprehensive related studies with interesting insights into exercise activity and personal healthcare physiology.

Limitations of the Study

Most advanced researches in sweat focused on the measurements in chemical species. In physical characteristics, secretory pressure may provide different insight of physiological health conditions yet it is lack of proper metrology methods. The main limitation of this study is that the correlation between disease and secretion pressure is still an underlying process. We can only presume this pressure intensity is related to psychological stress, inflammatory, immune, and nervous systems, but without precise verifications. We are looking forward to seeing this convenient, noninvasive sweat pressure measurement device provides a different vision and approach in understanding physical secretory characteristics and personal physiological health care.

Lead Contact

Bor-Ran Li, liborran@g2.nctu.edu.tw.

Materials Availability

This study did not generate new unique reagents.

Data and Code Availability

The published article includes all [datasets/code] generated or analyzed during this study.

METHODS

All methods can be found in the accompanying Transparent Methods supplemental file.

SUPPLEMENTAL INFORMATION

Supplemental Information can be found online at https://doi.org/10.1016/j.isci.2020.101658.

ACKNOWLEDGMENTS

This study was financially supported by the Ministry of Science and Technology (MOST) of Taiwan (108-2113-M-009 -016) and Center for Emergent Functional Matter Science of National Chiao Tung University, Featured Areas Research Center Program, within the framework of the Higher Education Sprout Project of the Ministry of Education (MOE) in Taiwan.

AUTHOR CONTRIBUTIONS

Dr. BR Li is the director of this project. PH Lin, WL Chang, and SC Sheu performed most experiments. PH Lin and WL Chang prepared the first drift and contributed equally to the paper as first authors.

DECLARATION OF INTERESTS

The authors declare no competing interests.

Received: August 19, 2020
Revised: September 11, 2020
Accepted: October 4, 2020
Published: November 20, 2020

REFERENCES

Anastasova, S., Crewther, B., Bembnowicz, P., Curto, V., Ip, H.M., Rosa, B., and Yang, G.-Z. (2017). A wearable multisensing patch for continuous sweat monitoring. Biosens. Bioelectron. *93*, 139–145.

Baker, L.B. (2017). Sweating rate and sweat sodium concentration in athletes: a review of methodology and intra/interindividual variability. Sports Med. *47*, 111–128.

Baker, L.B. (2019). Physiology of sweat gland function: the roles of sweating and sweat composition in human health. Temperature *6*, 211–259.

Bariya, M., Nyein, H.Y.Y., and Javey, A. (2018). Wearable sweat sensors. Nat. Electron. *1*, 160–171.

Choi, J., Ghaffari, R., Baker, L.B., and Rogers, J.A. (2018). Skin-interfaced systems for sweat collection and analytics. Sci. Adv. *4*, eaar3921.

Choi, J., Xue, Y., Xia, W., Ray, T.R., Reeder, J.T., Bandodkar, A.J., Kang, D., Xu, S., Huang, Y., and Rogers, J.A. (2017). Soft, skin-mounted microfluidic systems for measuring secretory fluidic pressures generated at the surface of the skin by eccrine sweat glands. Lab Chip *17*, 2572–2580.

Choi, J.-H., and Loftness, V. (2012). Investigation of human body skin temperatures as a bio-signal to indicate overall thermal sensations. Build. Environ. *58*, 258–269.

Christopher, H., and Gibbons, R.F. (2012). Primer on the Autonomic Nervous System, Third Edition (Academic Press).

Corrie, S.R., Coffey, J., Islam, J., Markey, K., and Kendall, M. (2015). Blood, sweat, and tears: developing clinically relevant protein biosensors for integrated body fluid analysis. Analyst *140*, 4350–4364.

Coyle, S., Morris, D., Lau, K.-T., Diamond, D., Taccini, N., Costanzo, D., Salvo, P., Di Francesco, F., Trivella, M.G., and Porchet, J.-A. (2009). Textile sensors to measure sweat pH and sweat-rate during exercise. Paper presented at: 2009 3rd International Conference on Pervasive Computing Technologies for Healthcare (IEEE).

Gao, W., Emaminejad, S., Nyein, H.Y.Y., Challa, S., Chen, K., Peck, A., Fahad, H.M., Ota, H., Shiraki, H., and Kiriya, D. (2016). Fully integrated wearable sensor arrays for multiplexed in situ perspiration analysis. Nature *529*, 509–514.

He, X., Xu, T., Gu, Z., Gao, W., Xu, L.-P., Pan, T., and Zhang, X. (2019). Flexible and superwettable bands as a platform toward sweat sampling and sensing. Anal. Chem. *91*, 4296–4300.

He, X., Yang, S., Pei, Q., Song, Y., Liu, C., Xu, T., and Zhang, X. (2020). Integrated smart janus textile bands for self-pumping sweat sampling and analysis. ACS Sens. *5*, 1548–1554.

Heikenfeld, J., Jajack, A., Feldman, B., Granger, S.W., Gaitonde, S., Begtrup, G., and Katchman, B.A. (2019). Accessing analytes in biofluids for peripheral biochemical monitoring. Nat. Biotechnol. *37*, 407–419.

Kumari, P., Mathew, L., and Syal, P. (2017). Increasing trend of wearables and multimodal interface for human activity monitoring: a review. Biosens. Bioelectron. *90*, 298–307.

Lan, L., Le, X., Dong, H., Xie, J., Ying, Y., and Ping, J. (2020a). One-step and large-scale fabrication of flexible and wearable humidity sensor based on laser-induced graphene for real-time tracking of plant transpiration at bio-interface. Biosens. Bioelectron. *165*, 112360.

Lan, L., Zhao, F., Yao, Y., Ping, J., and Ying, Y. (2020b). One-Step and spontaneous in situ growth of popcorn-like nanostructures on stretchable double-twisted fiber for ultrasensitive textile pressure sensor. ACS Appl. Mater. Interfaces *12*, 10689–10696.

Lee, H., Song, C., Hong, Y.S., Kim, M.S., Cho, H.R., Kang, T., Shin, K., Choi, S.H., Hyeon, T., and Kim, D.-H. (2017). Wearable/disposable sweat-based glucose monitoring device with multistage transdermal drug delivery module. Sci. Adv. *3*, e1601314.

Lin, C.-T., Kuo, S.-H., Lin, P.-H., Chiang, P.-H., Lin, W.-H., Chang, C.-H., Tsou, P.-H., and Li, B.-R. (2020). Hand-powered centrifugal microfluidic disc with magnetic chitosan bead-based ELISA for antibody quantitation. Sens. Actuator B Chem. *316*, 128003.

Lin, P.-H., and Li, B.-R. (2020). Antifouling strategies in advanced electrochemical sensors and biosensors. Analyst *145*, 1110–1120.

Liu, C., Xu, T., Wang, D., and Zhang, X. (2020). The role of sampling in wearable sweat sensors. Talanta *212*, 120801.

Liu, Y., Pharr, M., and Salvatore, G.A. (2017). Lab-on-skin: a review of flexible and stretchable electronics for wearable health monitoring. ACS Nano *11*, 9614–9635.

Livingston, R. (2010). Medical risks and benefits of the sweat lodge. J. Altern. Complement. Med. *16*, 617–619.

Nakata, S., Arie, T., Akita, S., and Takei, K. (2017). Wearable, flexible, and multifunctional healthcare device with an ISFET chemical sensor for simultaneous sweat pH and skin temperature monitoring. ACS Sens. *2*, 443–448.

Patel, S., Park, H., Bonato, P., Chan, L., and Rodgers, M. (2012). A review of wearable sensors and systems with application in rehabilitation. J. Neuro. Eng. Rehabil. *9*, 1–17.

Ranchordas, M.K., Tiller, N.B., Ramchandani, G., Jutley, R., Blow, A., Tye, J., and Drury, B. (2017). Normative data on regional sweat-sodium concentrations of professional male team-sport athletes. J. Int. Soc. Sport Nutr. *14*, 40.

Ray, T.R., Choi, J., Bandodkar, A.J., Krishnan, S., Gutruf, P., Tian, L., Ghaffari, R., and Rogers, J.A. (2019). Bio-integrated wearable systems: a comprehensive review. Chem. Rev. *119*, 5461–5533.

Sato, K., Kang, W., Saga, K., and Sato, K. (1989). Biology of sweat glands and their disorders. I. Normal sweat gland function. J. Am. Acad. Dermatol. *20*, 537–563.

Schazmann, B., Morris, D., Slater, C., Beirne, S., Fay, C., Reuveny, R., Moyna, N., and Diamond, D. (2010). A wearable electrochemical sensor for the real-time measurement of sweat sodium concentration. Anal. Methods *2*, 342–348.

Schulz, I.J. (1969). Micropuncture studies of the sweat formation in cystic fibrosis patients. J. Clin. Invest. *48*, 1470–1477.

Smith, C.J., and Havenith, G. (2011). Body mapping of sweating patterns in male athletes in mild exercise-induced hyperthermia. Eur. J. Appl. Physiol. *111*, 1391–1404.

Sonner, Z., Wilder, E., Gaillard, T., Kasting, G., and Heikenfeld, J. (2017). Integrated sudomotor axon reflex sweat stimulation for continuous sweat analyte analysis with individuals at rest. Lab Chip *17*, 2550–2560.

Taylor, C., Hardcastle, J., and Southern, K. (2009). Physiological measurements confirming the diagnosis of cystic fibrosis: the sweat test and measurements of transepithelial potential difference. Paediatr. Respir. Rev. *10*, 220–226.

Taylor, N.A., and Machado-Moreira, C.A. (2013). Regional variations in transepidermal water loss, eccrine sweat gland density, sweat secretion rates and electrolyte composition in resting and exercising humans. Extreme Physiol. Med. *2*, 4.

Temiz, Y., and Delamarche, E. (2018). Sub-nanoliter, real-time flow monitoring in microfluidic chips using a portable device and smartphone. Sci. Rep. *8*, 1–11.

Xia, Y., Zhang, H., Xu, L., Gao, Z., Zhang, H., Liu, H., and Li, S. (2018). An automatic cardiac arrhythmia classification system with wearable electrocardiogram. IEEE Access *6*, 16529–16538.

Yang, C.-H., Hsieh, Y.-L., Tsou, P.-H., and Li, B.-R. (2019). Thermopneumatic suction integrated microfluidic blood analysis system. PLoS One *14*, e0208676.

Yang, J., Wei, D., Tang, L., Song, X., Luo, W., Chu, J., Gao, T., Shi, H., and Du, C. (2015). Wearable temperature sensor based on graphene nanowalls. RSC Adv. *5*, 25609–25615.

Yang, Y., Song, Y., Bo, X., Min, J., Pak, O.S., Zhu, L., Wang, M., Tu, J., Kogan, A., and Zhang, H. (2020). A laser-engraved wearable sensor for sensitive detection of uric acid and tyrosine in sweat. Nat. Biotechnol. *38*, 217–224.

Yao, Y., Jiang, C., and Ping, J. (2019). Flexible freestanding graphene paper-based potentiometric enzymatic aptasensor for ultrasensitive wireless detection of kanamycin. Biosens. Bioelectron. *123*, 178–184.

Zheng, Y.-L., Yan, B.P., Zhang, Y.-T., and Poon, C.C. (2014). An armband wearable device for overnight and cuff-less blood pressure measurement. IEEE Trans. Biomed. Eng. *61*, 2179–2186.

iScience, Volume *23*

Supplemental Information

A Noninvasive Wearable Device for Real-Time Monitoring of Secretion Sweat Pressure by Digital Display

Pei-Heng Lin, Wei-Lun Chang, Sian-Chen Sheu, and Bor-Ran Li

Supporting information

A noninvasive wearable device for real-time monitoring of secretion sweat pressure by digital display

Pei-Heng Lin,[a,b,1] Wei-Lun Chang,[a,1] Sian-Chen Sheu,[a] Bor-Ran Li[a,b,c,d*]

[a]*Institute of Biomedical Engineering, College of Electrical and Computer Engineering, National Chiao Tung University, Hsinchu, Taiwan.*

[b]*Department of Electrical and Computer Engineering, College of Electrical and Computer Engineering, National Chiao Tung University, Hsinchu, Taiwan.*

[c]*Center for Emergent Functional Matter Science, National Chiao Tung University, Hsinchu, Taiwan.*

[d]*Lead Contact*

[1]*The authors contributed to this work equally*

*: *Corresponding author*
liborran@g2.nctu.edu.tw (BR Li)

Table. S1 Comparison of required sweat introduction time through regional variations in sweat rate. Related to Figure 4.

	Sweat Rate During Exercise ($mg \cdot cm^{-2} \cdot min^{-1}$)[a]	Secretion Volume ($\mu L \cdot min^{-1}$)	Required Sweat Introduction time (min)
Head	2.45	0.064	5.7
Back	1.658	0.044	8.5
Chest	1.403	0.037	10.0
Forearm	0.927	0.024	15.1
Upper arm	0.606	0.016	23.2

[a]Reference to **(Taylor and Machado-Moreira, 2013)**

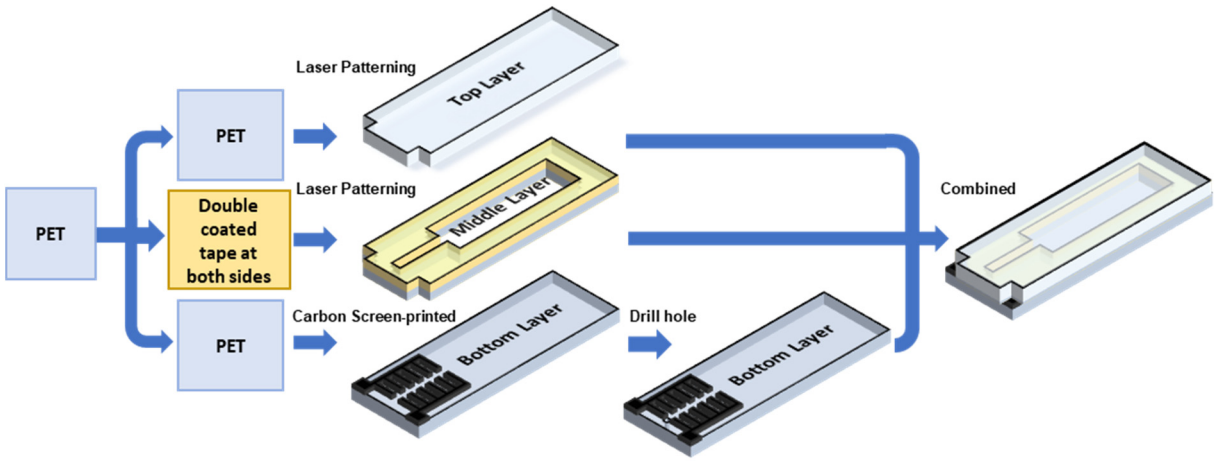

Figure S1 Fabrication process of each layer in the microfluidic chip. Related to Figure 1.

```
digitalWrite(5, LOW);    digitalWrite(4, LOW);
 delay(3800);
digitalWrite(5,LOW );  digitalWrite(4, HIGH);
 delay(200);
digitalWrite(5, LOW);    digitalWrite(4, LOW);
 delay(3800);
digitalWrite(5, HIGH);  digitalWrite(4, LOW);
 delay(200);
```

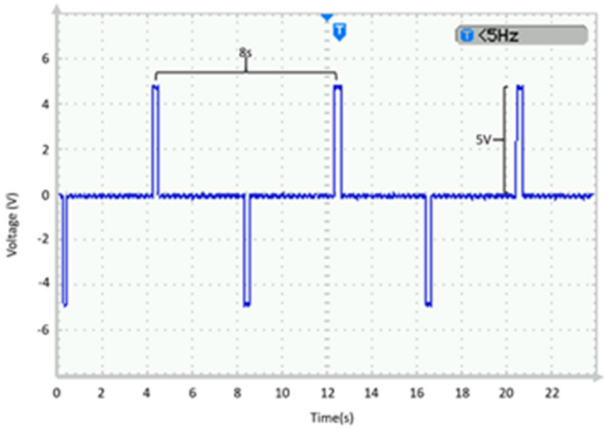

Figure S2 Applied source voltage to the electrode pairs. Related to Figure 2. The bipolar pulse wave with 2.5% duty cycle is implemented by digital writing; the demonstration was presented by a Beetle and an oscilloscope.

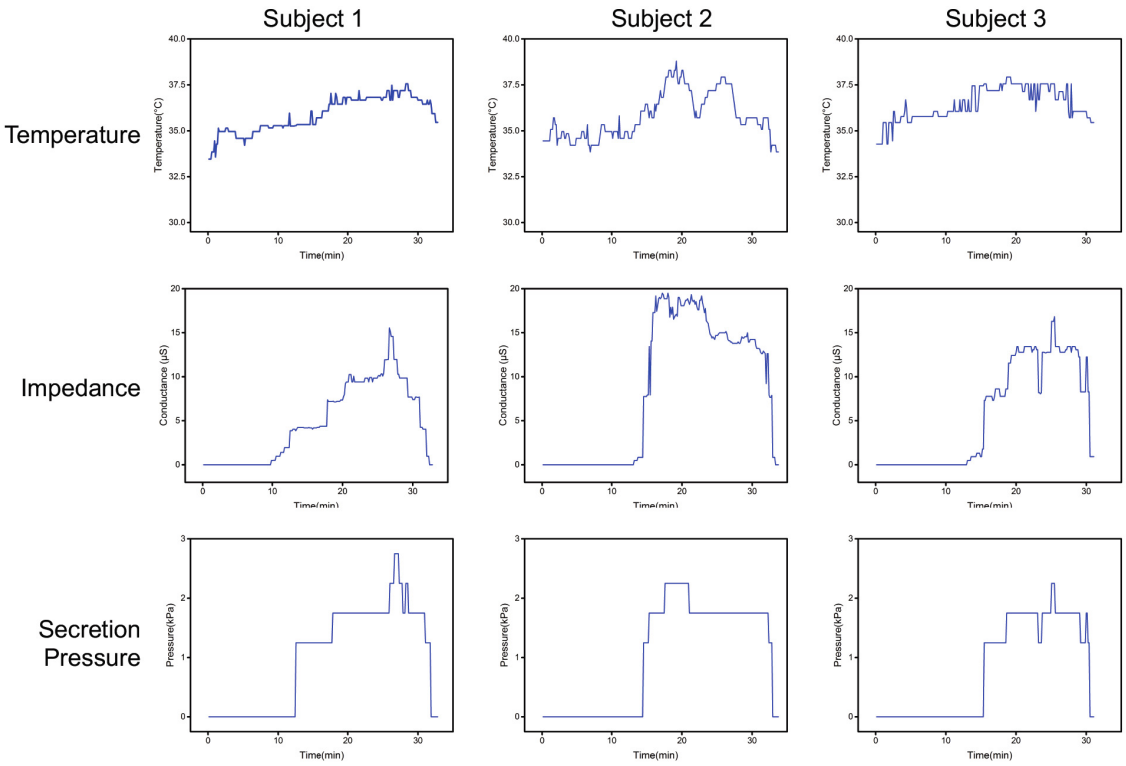

Figure S3 In situ measurements of wearable device during jogging. Related to Figure 5. Response signal shows the temperature, impedance and calculated secretion pressure.

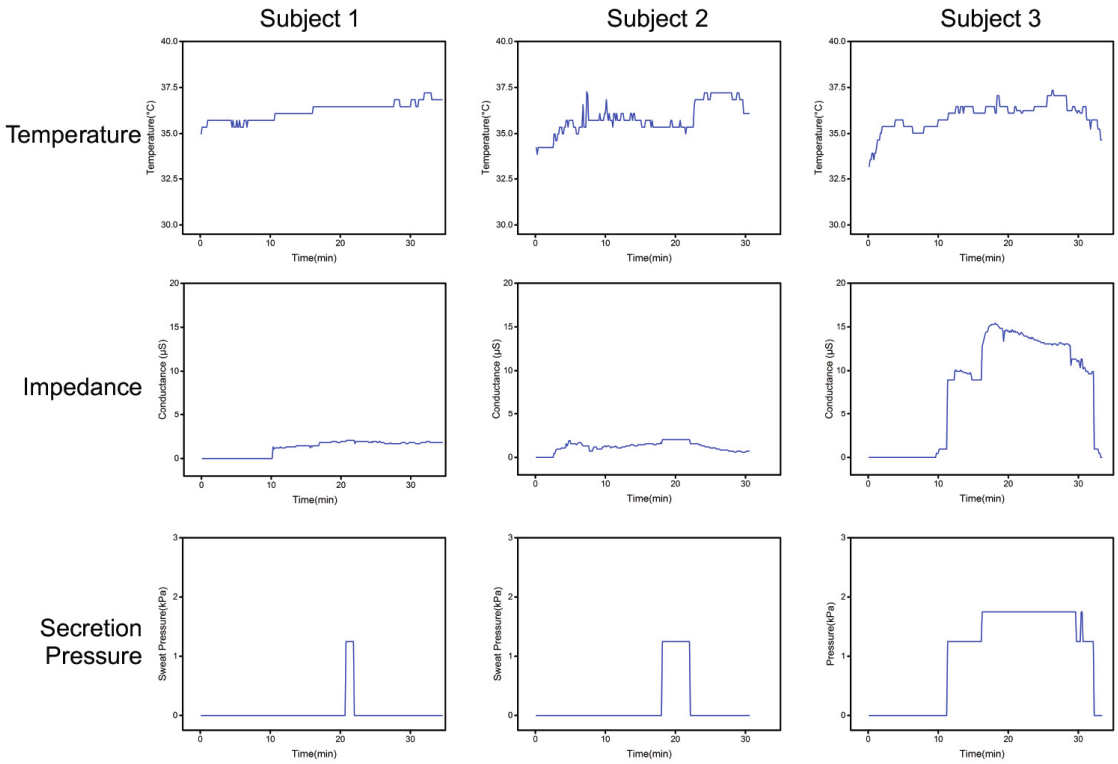

Figure S4 In situ measurements of wearable device during badminton. Related to Figure 5. Response signal shows the temperature, impedance and calculated secretion pressure.

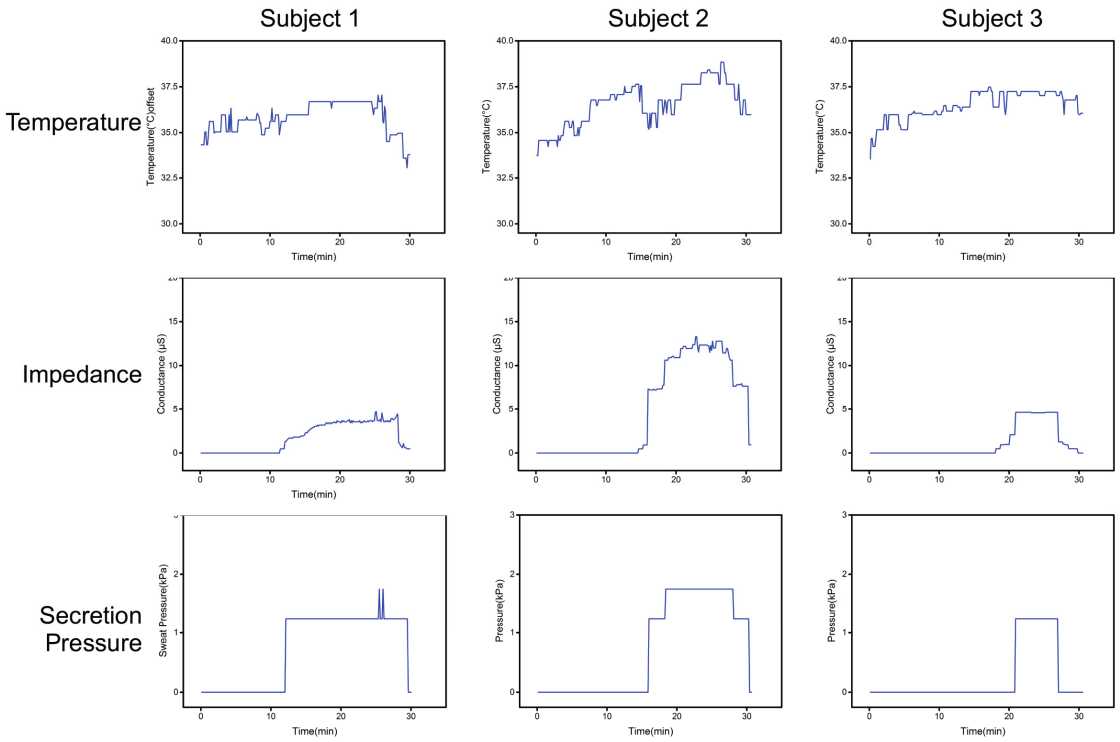

Figure S5 In situ measurements of wearable device during spinning bike. **Related to Figure 5.**

Response signal shows the temperature, impedance and calculated secretion pressure.

Transparent Methods

Capillary force interference in pressure measurement

As the movement of solution flows in or out of the microchannel, the capillary force might demonstrate interference in the outer pressure detection. If the channel characteristic is hydrophilic, additional capillary force would pull solution into the channel, resulting in the detected value being higher than the actual pressure. To further understand the equilibrium air–liquid interface state, an equation describing the applied pressure with capillary affected force is shown as

$$P_{app} = P_s - P_{capillary}$$

where P_{app} is the applied pressure that presents in the microfluidic channel, P_s is the air pressure inside the sealed chamber and the $P_{capillary}$ is the capillary force given from the Young–Laplace equation:

$$P_{capillary} = 2\sigma\, cos\theta(\frac{1}{d} + \frac{1}{w})$$

σ represents the surface tension of the sweat, w and d are the width and depth of the channel and the θ is the contact angle of the liquid. The contact angle of PET and sweat is 75° (experimental result), and the surface tension of sweat is calculated as 69.3 dyne· cm^{-1}. The width and depth of the microchannel are 1.4 and 0.2 mm, respectively. Based on equations (1) and (2), the capillary force is calculated approximately as 0.2 kPa, and the interference can be neglected in our system.

Sweat induction time through regional variations in predicting sweat rate during exercise

In this study, the wearable secretion pressure device is mounted on the forehead of human subjects. This system could be applied on other body parts in consideration of the sweat gland distribution in different region on human body. We calculated the sweat introduction time with regional sweat rate in Table S1, where the surface area of the sweat open to the first paired electrode in microchannel is 0.0263 cm^2 and the required volume of inlet channel is ~0.369 μL.

Materials and reagents

Sodium chloride, L-histidine monosodium phosphate, hydrogen chloride and sodium hydroxide were purchased from Sigma Aldrich (USA). The controlling pressure pump is a Mitos Pressure Pump from Dolomite (UK). Bluno Beetle is the Arduino microcontroller with Bluetooth 4.0 (BLE) purchased from DFRobot (China).

Fabrication of real-time sweat pressure sensing microfluidic chips

Chips were fabricated using 0.1 mm thick A4 size SCHMIDT PET Film. The SPCE electrode is in the width of 0.5 mm and the size of each comb is 2.25 mm in length and 0.5 mm in width (customized EPS Bio Technology Corp, Taiwan). Each PET layer is cut with a CO_2 laser cutting machine (3axle, Taiwan), the top layer pattern is cut under 10% power (6 W) and 20 mm/s speed. The channel layer (middle layer) is pretapped with the double coated tape on both sides of the PET film and subsequently cut by laser cutting machine under 10% power and 20 mm/s speed three times. The bottom layer is manufactured with screen-printed carbon electrodes. All the cutting and electrode patterns were designed with SolidWorks software. When the cutting process is done, we tear off the double coated tape and stick the three layers together. The outside of the chip is sealed by hot glue to make sure the chamber and channel in the chip are airtight. Finally, skin contact tape is drilled by a 1.5 mm punch and attached to the bottom layer of the chip using Epoxy resin (see Supporting information Figure S1).

Experimental setup for verification of microfluidic chip

Two experiments using a similar setup were designed and implemented to verify the versatility of the microfluidic chip in different environments. For the sweat-sodium test, we use two clips of poly(methyl methacrylate) to fix the microfluidic chip. A syringe containing artificial sweat was connected with microfluidic chip with a Teflon tube (Fluo-Tech, Taiwan). The liquid level was adjusted vertically to mimic different pressures, then the resistance response was observed to verify the microfluidic chip. The other experiment was the thermal test. To quantify the pressure value, we used a pressure pump (Mitos, Dolomite, UK) connected to a centrifuge tube (contain artificial sweat) instead of vertical movement of the syringe to mimic sweat pressure from gland pores. The microfluidic chip was placed on a hot plate to simulate different temperatures of the skin surface. When the pressure pump pressured the artificial sweat in the centrifuge tube and pushed liquid to wet each electrode tooth, the temperature

of the hot plate was adjusted, and the pressure value was displayed on the monitor. The data was recorded to plot a calibration curve from 25°C to 40°C to eliminate the effect of temperature change.

In situ measurement setup for real-time pressure detection

In order to keep the convenient and portable characteristic of real-time detection device, battery and transmitting device were placed in a PLA case fabricated by 3D printer (M200, Zortrax, Taiwan). The PLA case was fastened tightly on the outside of a head band with wire connected the temperature sensor and a microfluidic holder out of the case. The microfluidic holder was fabricated by double layers of PMMA pads with copper wire inlayed inside. Such design assists the connection and fixation for the displacement of disposable microfluidic chip. The temperature sensor and microfluidic holder and chip were placed on the inside area of the head band attached to the skin surface. In order to maintain the airtight and secretion fluid entrance, a skin-friendly, water-proof tape (Taicend, Taiwan) with a 1.8 mm diameter opening to the inlet of microfluidic channel. Except the microfluidic chip, the entire device is reusable. In addition, all the tests were obtained from healthy volunteers under the approving by ethics committee according to a protocol permitted by the Institutional Review Board (IRB) (NCTU-REC-108-083E).

Preparation of liquid samples

We prepared artificial sweat with different sodium concentrations with sodium chloride, L-histidine and monosodium phosphate according to international standard ISO105-E04. Deionized water was obtained using Direct-Q 3UV Water Purification. Artificial sweat with 0.06%, 0.257% and 0.525% weight percentage concentrations of sweat-sodium was prepared according to a previous study(Baker, 2017). For example, sodium ions of a 0.06% weight percentage concentration of artificial sweat were approximately 41 millimolar (41 mM). The solution was prepared with 20 g of deionized water, 12 mg of sodium chloride (Sigma Aldrich, USA), 10 mg of L-histidine (Sigma Aldrich) and 44 mg of monosodium phosphate (Sigma Aldrich). The difference between the 0.06%, 0.257% and 0.525% weight percentage concentrations of artificial sweat is only the sodium chloride weight, 12 mg, 51.4 mg and 105 mg, and the other components are the same. After the different concentrations of artificial sweat are prepared, the pH is adjusted by adding 1N hydrogen chloride (Union Chemical Works LTD.,

Hsinchu, Taiwan) and 1N sodium hydroxide (Union Chemical Works Ltd.). All solutions were prepared and used at room temperature.

Implementation of Arduino-based electronic devices and Arduino code for resistance measurement

Bluno Beetle is the smallest Arduino microcontroller with Bluetooth 4.0 (BLE) from DFRobot (China). Since the results coming out of the mobile app are processed by Beetle BLE, calculations were done by the code written into Arduino system. The code running on the Beetle was written using the Arduino IDE (v1.8.8) software, and it helps receive data from sensors. Among both sensors, "TMP36G" voltage temperature sensors detect body temperature with its pin V_S, V_{OUT}, GND connected to 5 V, analog read, GND pins in Beetle, and the result is calculated by the datasheet of TMP36G. The unknown resistance across an electrode pair was calculated using the voltage division method with an 8.2k resistor and microfluidic chip in series with a pulse-width bipolar voltage to provide power. The pulse-width bipolar voltage was set up using digital writing to produce pulses at both sides, in turn; therefore, the electrochemical reaction in the microfluidic chip can be highly diminished and extend the working duration. Since the cycle time of positive pulses is 8 seconds, the voltage value of the microfluidic chip was detected every 8 seconds (see Supporting information Figure S2).

Supplemental reference

Baker, L.B. (2017). Sweating rate and sweat sodium concentration in athletes: a review of methodology and intra/interindividual variability. Sports Medicine *47*, 111-128.

Taylor, N.A., and Machado-Moreira, C.A. (2013). Regional variations in transepidermal water loss, eccrine sweat gland density, sweat secretion rates and electrolyte composition in resting and exercising humans. Extreme physiology & medicine *2*, 4.